SUPPLEMENTAL MATERIAL

Index

Methods: Simulation of Force Clamp Experiment

The microtubule assembly dynamics simulation as developed by VanBuren *et al*. [1, 2] was adapted to simulate assembly under load, applied by laser tweezers in a microfabricated chamber. In general, this required updating the model to include (1) assembly of a thermally-driven microtubule under compressive loading in the presence of a rigid barrier, and (2) simulation of the data collection via bead tracking. All additional simulation parameters and methods are as described previously [1, 2]. Similar to previous work, it was assumed that all microtubules had 13 protofilaments in a B-lattice.

Simulation Coordinate System and Variables

In order to simulate the experimental assay and data collection method, a coordinate system was defined such that the bead, optical trap, and fabricated barrier positions could be tracked relative to length changes of the simulated microtubule (Table S1, Figure S1).

Table S1: Coordinate System and Simulation Variables

Variable	Description	Definition
x	Axis along length of microtubule	x=0 at microtubule minus-end
x_{wall}	Position of microfabricated wall	x_{wall} = x distance from microtubule minus-end to wall
$L_{pf,i}$	Length of protofilament	$L_{pf,i}$ = x distance from microtubule minus-end to tip of each individual protofilament (i=1 to 13)
L_{MT}	Length of microtubule	L_{MT} = x distance from microtubule minus-end to the tip of the longest protofilament at the plus-end
$L_{gap,i}$	Gap between individual microtubule protofilament tips and the microfabricated wall	$L_{gap,i}$ = x distance from individual protofilament tips (i =1 to 13) to microfabricated wall
x_{trap}	Position of optical trap	x_{trap} = x distance from microtubule minus-end to center of trap
x_{bead}	Position of microtubule-attached bead	x_{bead} = x distance from microtubule minus-end to center of bead

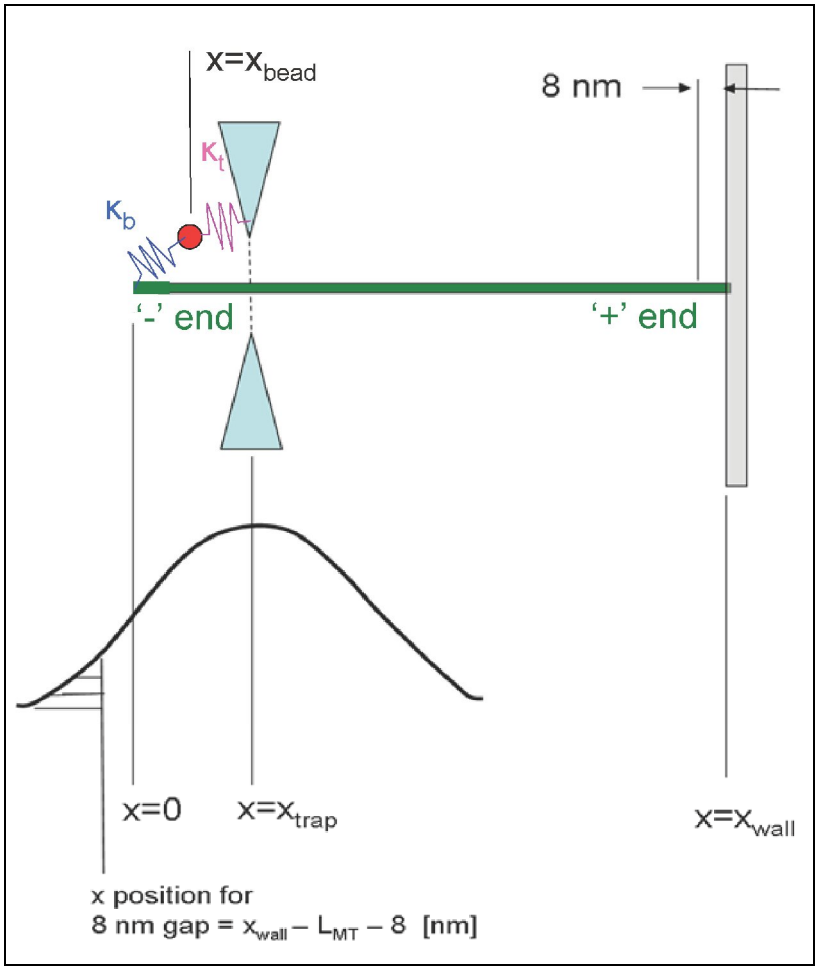

Figure S1: Coordinate system for simulation of microtubule dynamics under compressive load. The frame of reference is the microtubule, with the origin at the point of bead attachment (i.e. the minus end). For simplicity, the situation depicted here is for the lead protofilament, which requires an 8 nm gap to open up to allow tubulin subunit addition. Lagging protofilaments will require smaller gaps, and if they trail the lead protofilament by more than 8 nm, then they do not require a gap at all and so are unaffected by the presence of the wall. See text for further details.

In this system, the microtubule-bead complex moves relative to the wall as a result of the optical force and thermal forces. The frame of reference chosen here is the microtubule with the origin chosen to be at the point of bead attachment, which is referred to for simplicity as the "minus end", even though the microtubule in practice extends beyond the attachment point. However, this minus-end extension does not affect the force balance calculation, and it is the length changes at the plus end that are of interest in the simulation and experiment. The minus end defines the origin in the coordinate system, and positive values of x are in the direction of the plus end of the microtubule. As a result of thermal fluctuations, the wall is almost always further from the origin than the plus end of the microtubule ($x_{wall} > L_{MT}$), although strictly speaking if the leading protofilament is transiently in direct contact with the wall, then $x_{wall} = L_{MT}$. We considered the microtubule to be incompressible so that x_{wall} can never be less than L_{MT}. The variables listed in Table S1 are shown in Figure S1 relative to the position of the growing microtubule (green). A bead (red) is attached via a linear spring (blue) to the microtubule (green) at x=0, which is stretched to a position $x = x_{bead}$ by the optical force on the bead. An optical trap (cyan) centered at $x = x_{trap}$ acts as a linear spring (magenta) to apply a force on the microtubule in the direction of the barrier and constrain bead movement relative to the microtubule. Together, the trap stiffness (κ_t, magenta) and the bead linkage stiffness (κ_b, blue) define a series compliance that elastically links the optical trap to the microtubule minus end to create a harmonic potential well in the x-direction. If the trap center is displaced from the minus end ($x_{trap}>0$), then there is an elastic force on the microtubule that pushes the microtubule toward the wall. Addition of a tubulin subunit at the plus-end of an individual microtubule protofilament requires that

the gap between the wall and the i^{th} protofilament ($L_{gap,i}$) is large enough to allow an ~ 8 nm tubulin dimer to enter (shown in Figure S1 as 8 nm gap). Each protofilament has a length $L_{pf,i}$ and the length of the microtubule is defined as $L_{MT}=\max(L_{pf,i})$. The gaps between the individual protofilament tips and the wall open up as a result of thermal forces that drive the microtubule away from the wall, thus allowing polymerization under compressive load.

Simulation of Microtubule Assembly Under Load

In order to simulate microtubule assembly as the tip of the microtubule is forced against the microfabricated barrier via the bead/trap linkage, the probability of a gap opening up between the barrier and the tip of each microtubule protofilament that is large enough to add a tubulin dimer is calculated. For a thermally-driven spring, the probability density function obeys a Gaussian, which is experimentally observed for optical traps [3, 4]. In the simulation, the Gaussian has mean = x_{trap}, and variance

$$\sigma^2 = k_B T / \kappa_{effective} \qquad (1)$$

where $\kappa_{effective}$ is the effective spring constant of the bead/trap microtubule linkage. The effective spring constant of the bead/trap microtubule linkage is calculated based on two springs connected in series, and is given by

$$\kappa_{effective} = \kappa_b \kappa_t / (\kappa_b + \kappa_t) \qquad (2)$$

where κ_b is the spring constant of the bead/microtubule linkage, and κ_t is the spring constant of the bead in the trap.

Via random sampling from the Gaussian probability density function, the stochastic effect of gap opening probability on the event time for individual tubulin

heterodimer addition (by protofilament) is then calculated. The probability that the i^{th} protofilament will be at least a distance of 8 nm from the wall is given by

$$p_i = \frac{\int_{-\infty}^{x_{wall}-L_{pf,i}-8nm} f(x)dx}{\int_{-\infty}^{0} f(x)dx} \qquad x_{wall}\text{-}L_{pf,i} \le 8 \text{ nm} \qquad (3)$$

$$p_i = 1 \qquad x_{wall}\text{-}L_{pf,i} > 8 \text{ nm} \qquad (4)$$

where f(x) is the Gaussian probability density function with mean x_{trap} and variance σ^2 (as described above). The event time for each protofilament, t_i, is then calculated using

$$t_i = -ln(rand)/(p_i\, k^*_{on}) \qquad (5)$$

where k^*_{on} is the pseudo first-order rate constant for tubulin addition to the protofilament tip when there is no barrier ($k^*_{on}=k_{on}$[GTP-tub]), and *rand* is a uniformly distributed, uncorrelated random number over the range 0 to 1. These event times are then used as described by VanBuren *et al* [1, 2] to stochastically simulate microtubule assembly, with model parameters as listed in Table S2 and described previously.

Table S2: Model Parameters

Parameter	Description	Value
[GTP-tub]	Free GTP-Tubulin concentration	5.3×10^{-6} M
k_{on}	Tubulin on-rate constant	4×10^{6} $M^{-1}sec^{-1}$
$k_{hydrolysis}$	Hydrolysis rate constant	0.95 sec^{-1}
ΔG^{0*}_{Long}	Longitudinal chemical bond energy (tubulin polymer)	-6.8 k_BT
ΔG^{0}_{Lat}	Lateral chemical bond energy (tubulin polymer)	-5.7 k_BT
κ_b	Spring constant for bead-microtubule linkage	0.021 pN/nm
κ_t	Spring constant for trap	0.021 pN/nm
T	Temperature	309 K

Simulation of Data Collection via Bead Tracking

In order to accurately reproduce experimental observation conditions, bead positions are simulated and updated every 0.2 ms. The procedure for this update is as follows:

a) The probability density function (mean= x_{trap}, variance calculated via $\kappa_{effective}$, as described above) of possible microtubule minus-end positions is randomly sampled, to account for microtubule diffusion away from the wall in the potential well defined by the optical trap (positions where $x<0$).

b) Then, given the microtubule minus-end position and the trap position, a "rest" position of the bead is calculated. The entire (Gaussian) probability density function of available bead positions relative to the microtubule tip is then randomly sampled using a probability density function with the mean equal to the calculated "rest" position of the bead and the variance calculated via $\kappa_{effective}$, as described above.

c) Finally, error in bead measurement by the microscope-quadrant photodetector system was accounted for by adding Gaussian white noise with mean zero and standard deviation equal to the experimentally measured error in bead location (1 nm).

Finally, the simulation accounted for trap position reset (every 100 ms, used to maintain force clamp). In the case of a set point force (F), the trap position was reset every 100 ms (i.e. at 10 Hz) in the simulation according to:

$x_{trap} = F/\kappa_t + mean(x_{bead,j})$ *for j=1:500* (6)

where j is the index of the last 500 observations obtained at 5 kHz. This resets the simulation such that trap location is set to a new position that is x_{trap} nanometers in front of the bead, so that the trap moves along with microtubule assembly, and disassembly, as it occurs at the plus end of the microtubule. We found that the mechanical energy minimization routine used in VanBuren et al. [1], which is the slowest part of the algorithm, could be turned off without significantly altering the tip structure or simulation output. In our previous study [1], we found that there was little curling during the growth phase, consistent with our findings here. Therefore, for the sake of speed, we simulated without mechanical energy minimization.

Results: Raw data (5 kHz) temporally filtered to force clamp resolution (10 Hz)

The force clamp routine averages the 5 kHz data stream and updates the position of the force clamp at a rate of 10 Hz, with the result that each update is based on 500 individual bead position measurements. To illustrate the effect of temporal averaging, we show an example trace in Figure S2 (below) where both panels show full 5 kHz data streams (gray) and low-pass filtered streams (software implemented, 5^{th} order low-pass filter, 10 Hz cutoff, black) with the only difference being the amount of data presented. Variability is evident in the trace filtered to match force clamp resolution, though the absence of the force clamp results in underestimation of microtubule length changes.

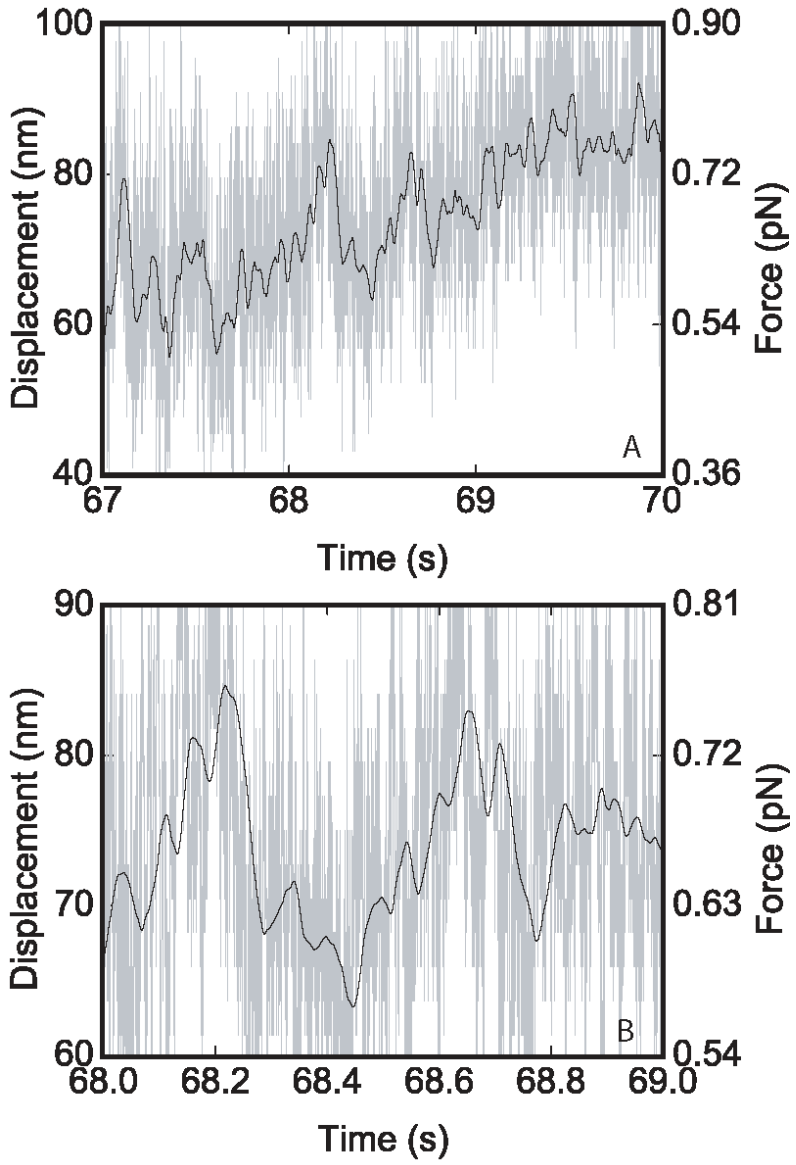

Figure S2: Low pass filtered stationary trap data demonstrating that variability in growth is evident in raw data taken with a stationary trap. The lower trace shows a subset of the data from the upper trace.

Results: Additional traces of force clamp experimental data

All experimental data traces filtered at 10 Hz are sorted by force clamp value and summarized below.

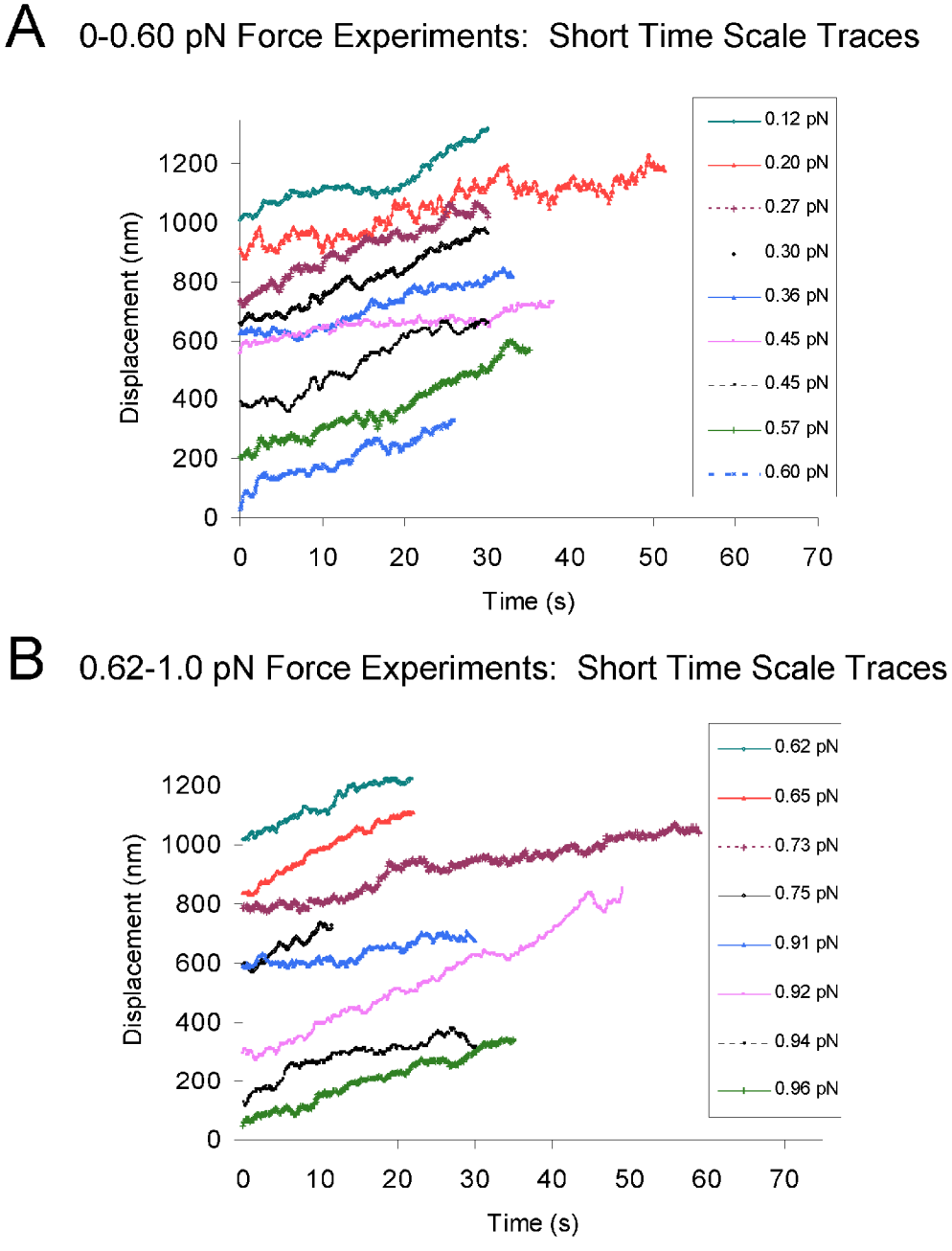

Figure S3: (A) Experimental microtubule length-time traces for short observation time 0-0.60 pN force clamp experiments. Traces are organized by force value, with lowest

forces in the upper portion of the graph, and higher forces in the lower portion of the graph. (B) Experimental microtubule length-time traces for short observation time 0.62-1.0 pN force clamp experiments. Traces are organized by force value, with lowest forces in the upper portion of the graph, and higher forces in the lower portion of the graph.

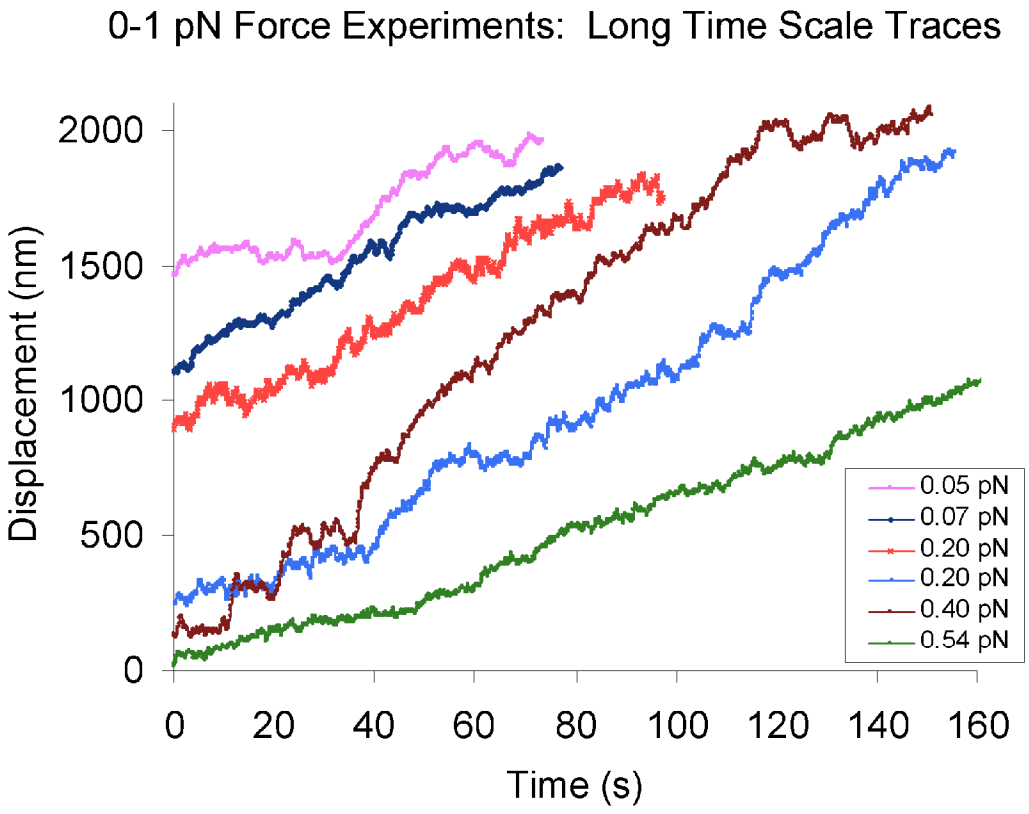

Figure S4: Experimental microtubule length-time traces for long observation time 0-1 pN force clamp experiments. Traces are organized by force value, with lowest forces in the upper portion of the graph, and higher forces in the lower portion of the graph.

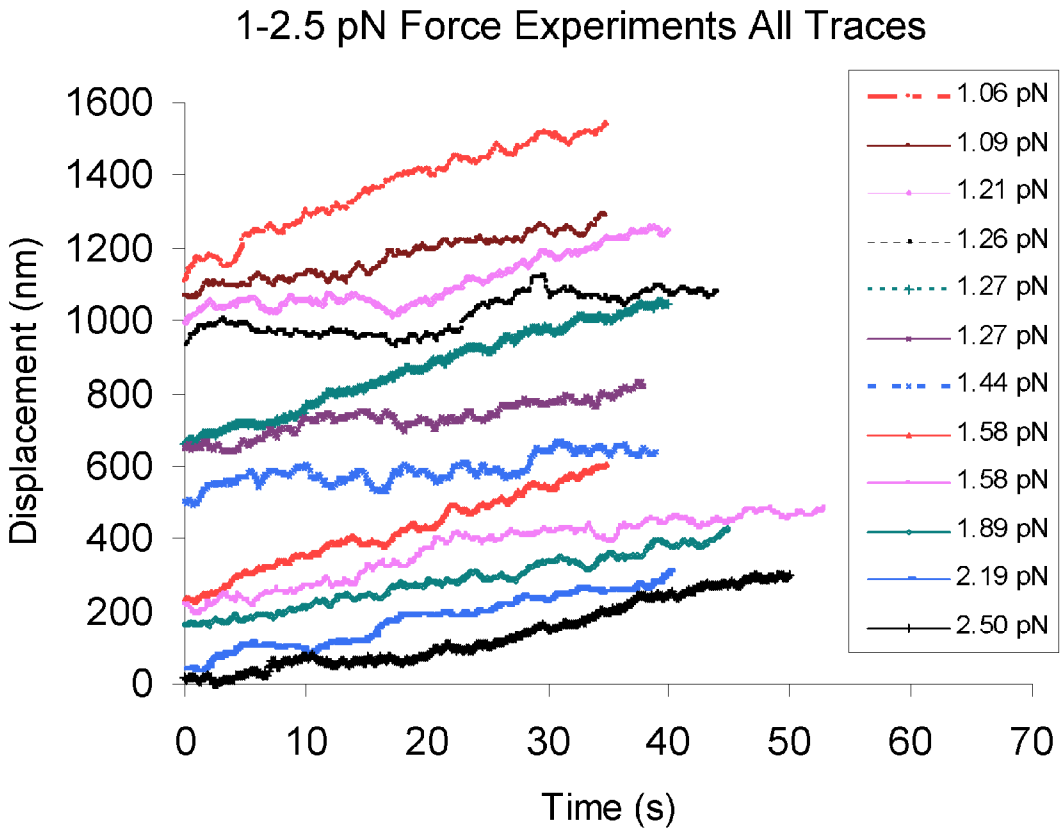

Figure S5: Experimental microtubule length-time traces for 1.0 – 2.5 pN force clamp experiments. Traces are organized by force value, with lowest forces in the upper portion of the graph, and higher forces in the lower portion of the graph.

Results: Example of apparent steps at low resolution

Figure S6 shows an example of data that appears to be stepwise growth when viewed at the 25 Hz data rate of Kerssemakers *et al* [5], but is revealed to be rapid continuous growth at higher bandwidth (500 Hz). Similar to the data presented by Kerssemakers *et al* [5] , these data were taken using a stationary trap. For the most part we relied on the force clamp to eliminate the effect of the series compliance while Kessermakers *et al.* first measured the compliance of the linkage and then corrected for it.

Hence, the changes in bead displacement shown in Figure S6 reflect the microtubule length changes but underestimate their actual value. However, we can still use the high bandwidth data produced in stationary trap records to look for the appearance of stepwise growth by the addition of tubulin oligomers. In the left panel, low-pass filtered data (cut off=25 Hz, 5th order, software implemented Butterworth low-pass filter) is shown resampled to 25 Hz (black trace with diamond markers) and super-imposed on data filtered with a 500 Hz cut-off (gray trace without markers). In this presentation, a step of ~20 nm is apparent in the filtered and resampled data. In the right panel, the portion of the higher bandwidth data (500 Hz cutoff) that contains the apparent step is shown on a longer x-axis. In this higher time resolution presentation, it is clear that this step is actually a period of fast microtubule growth. This analysis merely serves as an example showing how data processing or low bandwidth acquisition might lead to misinterpretation of a period of high speed growth as a stepwise addition to the polymer.

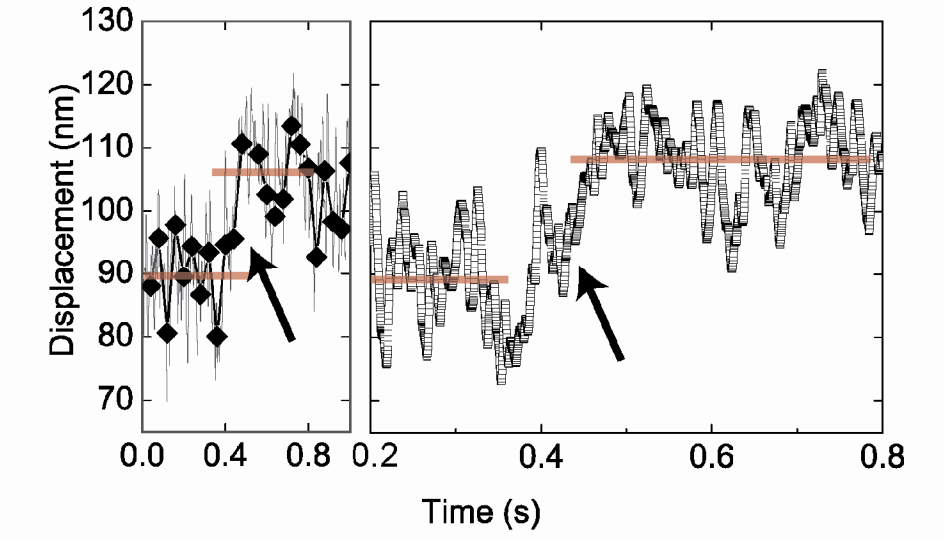

Figure S6: Data averaging produces the appearance of step-wise growth which at higher time resolution is shown to be a period of rapid, continuous growth.

Results: Lateral cap model simulations

A numerical model for microtubule dynamic instability that relied on a single layer of GTP-tubulin was previously developed by Bayley and coworkers [6, 7]. Termed the "Lateral Cap" model, this simulation assumed direct coupling of GTP-tubulin hydrolysis with addition of new tubulin subunits at the terminal end of a growing microtubule. Thus, a single layer of GTP-tubulin subunits in Lateral Cap model simulations could qualitatively account for the dynamic instability behavior of microtubules. Subsequently, further analysis of this model by Odde and coworkers [8] verified that qualitative dynamic instability behavior could be reproduced by this model, including periodic deviations from linear growth. In order to compare results from the lateral cap model simulation for microtubule dynamic instability with our nanoscale experimental data, we ran simulations of dynamic instability using FORTRAN code that had been previously developed [8], and then added Gaussian white noise (mean = 0, standard deviation = 1 nm) to account for the experimental error in nanoscale microtubule length measurement. We then compared multiple time-step growth and shortening excursion lengths for nanoscale dynamic instability as predicted by the lateral cap model to experimental data for nanoscale excursion lengths (Figure S7). We find that the blunt microtubule tip structure predicted by the single-layer GTP-cap model cannot account for the wide range of nanoscale growth fluctuations during microtubule assembly. Here, GTP-tubulin hydrolysis coupled to the distal addition of new tubulin subunits predicts a narrow range of growth and shortening excursions, similar to GMP-CPP stabilized microtubules.

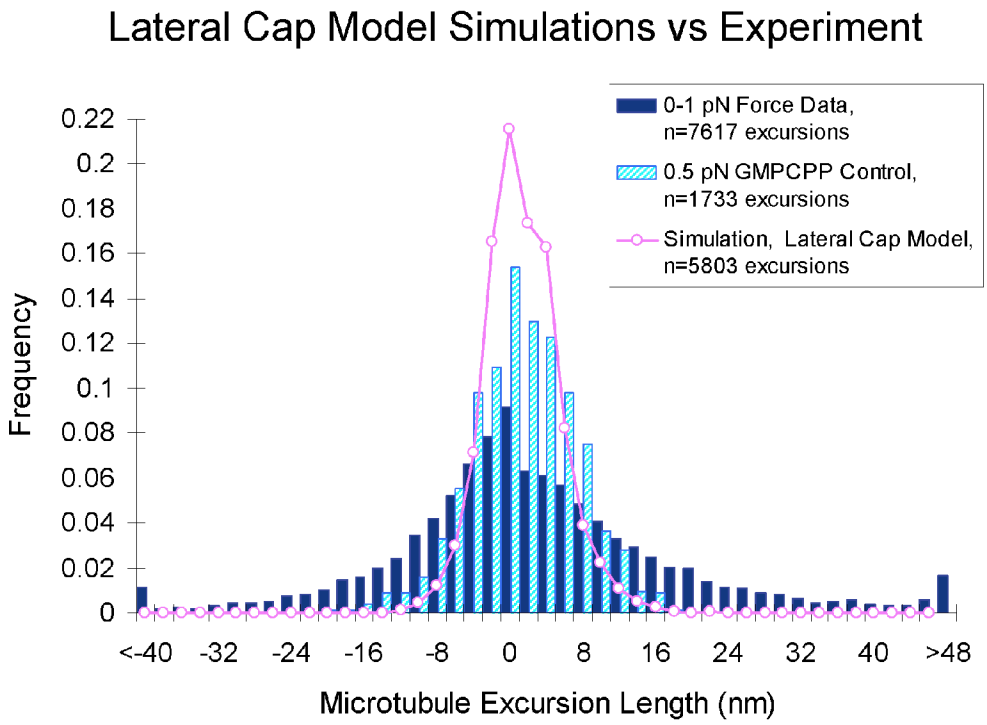

Figure S7: Lateral Cap model simulations as compared to nanoscale experimental microtubule assembly data. The single-layer lateral GTP-cap model is unable to account for the large fluctuations in nanoscale microtubule assembly that are observed experimentally.

Discussion: Assay variability in relation to growth-phase shortening events

Alternative explanations for the observed growth phase variability are most broadly rejected by the stable microtubule control data (main text; Figure 5, Table 2). The microtubule length standard deviation for GMP-CPP controls of 3.5 nm at measurement intervals of 0.1 second was, as expected, greater than that found when tracking a bead affixed to the coverslip surface ($\pm$1.5 nm, data not shown). The larger variation is principally due to increased thermal motion, but slow lengthening and shortening may contribute since the microtubule cannot be guaranteed to be entirely stable. Indeed, occasionally GMP-CPP microtubules were seen to exhibit very slow length changes that eventually became large enough for observation by DIC microscopy.

In addition to the relatively stable GMP-CPP microtubule control, physical arguments also reject likely alternate explanations: 1) the optical tweezers force clamp is unstable and as a result produces the perceived lengthening and shortening events, 2) the barriers themselves are sufficiently rough that the microtubule appears to shorten and lengthen as the tip moves about the surface and 3) microtubule bending fluctuations are large enough to make the microtubule appear to shorten and lengthen. In addition to the GMP-CPP controls showing that none of these possibilities is in fact an issue, each one can also be eliminated by further arguments.

In the case of the optical tweezers stability, tracking a bead attached to the surface of the coverslip demonstrates that the tweezers, and the routines that operate them, are capable of tracking a bead's position with an error of $\pm$ 1.5 nm (data not shown). This error is the result of the cumulative error of small air currents inside the optical tweezers enclosure, which cause very small error signals on the detector, and more significantly

the fact that the bead was not perfectly immobilized but was capable of small movements while attached to the coverslip.

Simple physical arguments show that barrier roughness cannot be responsible for the shortening events. Imagine a rough barrier with several pits or crevices into which a microtubule can slide and remain. In some cases, as the microtubule grows, the tip will slip out of a local pit and the compressive force of the trap will push the microtubule down into the next minimum, eventually reaching a stable crevice. These events would then appear to be shortening. There are two fundamental arguments that reject this mechanism. First, the viscoelastic relaxation time of the microtubule-bead in the trap is ~2 msec. If the microtubule slipped from one crevice to a lower one, the travel time for the bead from its first equilibrium position to the lower would be of the order of the relaxation time. Since the force clamp routine updates every 100 msec, this event would appear as a sudden drop from one position to the next with a time interval of one update. This has never been observed in any of the records; all shortening events happen at speeds similar to growth: less than 50 nm/s.

A second argument starts with the observation that at some point the microtubule would reach a global minimum in the rough landscape. From there, it would first have to make an excursion from the minimum, against load, and then slip past the rough obstruction back to a new local minimum. At a typical clamping force of ~ 1.5 pN the energy necessary to work against the compressive force to a distance of 40 nm would be 60 pN-nm or equivalently ~15 k_BT, which from the Boltzmann distribution corresponds to a probability of ~10^{-7}. Dividing this probability into the correlation time of the trap, 1-4 msec, predicts the observation time necessary to see a single such event as 10000-

40000 seconds, whereas in the experiments microtubules were observed for a total of 1,676 s. Shortening events are far more frequent than this and so must arise from another source.

Furthermore, each experiment began by guiding the microtubule tip into the microfabricated vertex where it would abut the microfabricated barrier by sliding the microtubule along the barrier wall. In no case was a stick-slip behavior observed during this process. Additionally, each observation began with a substantial observation in a stationary trap that usually achieved high force. These observations again produced no evidence of the microtubule sticking and slipping past a rough area in the barrier.

Finally, the possibility that the microtubule is changing shape on a time scale and in a fashion that could create the appearance of lengthening and shortening can be eliminated. Following Gittes and Howard [9], the first bending mode of a 5 μm microtubule would have a characteristic relaxation time on the order of 100 μs with the higher order mode relaxation times decreasing according to the inverse fourth power of the mode number. Microtubule shape fluctuations would therefore be heavily averaged because the force clamp is updated infrequently, once every 100 ms, equivalent to 1000 times the slowest viscoelastic relaxation time of the microtubule during thermally-driven bending. Accounting for the large variation in the reported flexural rigidity of microtubules [1], a worst case estimate of the relaxation time might be 20 times greater, but still far too short to be apparent in the force clamping records. Similarly, the motion that one would expect from compression of the microtubule due to thermal motion is quite small. Assuming that a microtubule wall is an isotropic material, one can calculate the elastic modulus from the flexural rigidity [1, 9]. Conservative estimation of the elastic

modulus indicates that 5 pN would result in compression of much less than 1 nm. In addition, Kerssemakers *et al*. [5] considered the thermal fluctuations of protofilament extensions at the end of the microtubule, and estimated that such extensions are still very stiff and would only fluctuate a few nanometers at most.

A further consideration is the lack of thermodynamic stability of mechanically compliant structures. While it is formally possible for a single protofilament to protrude beyond the other protofilaments, it is very unstable. Using our base parameter set, we estimate that the mean lifetime of single subunit with no lateral neighbors is ~0.2 ms. By contrast the mean arrival time for an incoming subunit is about 50 ms. So the probability of adding another subunit onto one that lacks lateral neighbors is 0.004. Further addition without loss, necessary for building up a single protofilament extension, is even less likely. For example, in the case of 4 tubulin subunits (32 nm long protofilament extension), the mean time for one of the 4 longitudinal bonds to break is ~50 μs. Therefore, we conclude that these structures will rarely occur, and if they do they will be extremely short-lived. Of course a two-protofilament extension could occur, as in Fig. 2E, but these are also very unstable, and in the simulation usually results in catastrophe. Even a two-protofilament extension that is 8 subunits long (64 nm) will be unlikely to buckle significantly. For example, given elastic modulus E=260 pN/nm^2 [1], and second moment of inertia of the cross-sectional area I=[(4 nm)^3(8 nm)]/12 = 43 nm^4, then the Euler critical buckling force is

$$F^0_{c,2pf} = \pi^2 EI \big/ L^2 = 27pN \tag{7}$$

which is well below the maximum force of 2.5 pN used in this study (note that much of the data were collected at 0-1 pN). Accounting for thermal effects on the buckling will

have only a modest effect on the predicted buckling force, since the length of the projection (L=64 nm) is small compared to the persistence length of the projection (L_p=EI/kBT=2600 nm). For the single protofilament extension (L=32 nm), the persistence is similarly large (L_p=510 nm), so that in neither case are thermal forces expected to play a significant role. In either case, (one or two protofilaments of 32 or 64 nm, respectively) the critical buckling force is still much more than the ~5 pN required to buckle the entire microtubule. Note that microtubule buckling was not observed at the forces used in this study (max 2.5 pN). Furthermore, the fluctuations were largely uncorrelated with the load, and were in fact *larger* in the low force experiments than in high force experiments, which is the opposite of what one might expect if the applied load were inducing structural changes in the tip. Finally, it is important to note that the manipulation system is very soft in the direction away from contact with wall, and very stiff when in contact with the wall. From Boltzmann's Law, this implies that the microtubule tip rarely contacts the wall, and so is unable to sustain deformed tip states. Therefore, neither thermal events nor the forces exerted in these studies would produce significant tip deformation.

Supplemental References

1. VanBuren, V., Cassimeris, L., and Odde, D.J. (2005). Mechanochemical model of microtubule structure and self-assembly kinetics. Biophys J *89*, 2911-2926.
2. VanBuren, V., Odde, D.J., and Cassimeris, L. (2002). Estimates of lateral and longitudinal bond energies within the microtubule lattice. Proc Natl Acad Sci U S A *99*, 6035-6040.
3. Ashkin, A. (1998). Forces of a single-beam gradient laser trap on a dielectric sphere in the ray optics regime. Methods Cell Biol *55*, 1-27.
4. Block, S.M. (1992). Making light work with optical tweezers. Nature *360*, 493-495.
5. Kerssemakers, J.W., Laura Munteanu, E., Laan, L., Noetzel, T.L., Janson, M.E., and Dogterom, M. (2006). Assembly dynamics of microtubules at molecular resolution. Nature *442*, 709-12.
6. Bayley, P., Schilstra, M., and Martin, S. (1989). A lateral cap model of microtubule dynamic instability. FEBS Lett *259*, 181-184.
7. Bayley, P.M., Schilstra, M.J., and Martin, S.R. (1990). Microtubule dynamic instability: numerical simulation of microtubule transition properties using a Lateral Cap model. J Cell Sci *95 (Pt 1)*, 33-48.
8. Odde, D.J., Buettner, H.M., and Cassimeris, L. (1996). Spectral analysis of microtubule assembly dynamics. AIChE Journal *42*, 1434-1442.
9. Gittes, F., Mickey, B., Nettleton, J., and Howard, J. (1993). Flexural rigidity of microtubules and actin filaments measured from thermal fluctuations in shape. J Cell Biol *120*, 923-934.